arXiv:1607.04999v2 [cond-mat.mes-hall] 13 Oct 2016

Intervalley scattering in MoS_2 imaged by two-photon photoemission with a high-harmonic probe

R. Wallauer,[1] J. Reimann,[1] N. Armbrust,[1] J. Güdde,[1] and U. Höfer[1]

[1]*Fachbereich Physik und Zentrum für Materialwissenschaften, Philipps-Universität, 35032 Marburg, Germany*

(Dated: October 14, 2016)

Abstract

We report on the direct mapping of electron transfer in the momentum space of bulk MoS_2 by means of time- and angle-resolved two-photon photoemission with a high-harmonic probe. For this purpose, we have combined a high-repetition rate high-harmonic source with tunable femtosecond pump pulses and a 3D (k_x, k_y, E) electron spectrometer. We show that optical excitation slightly above the A exciton resonance results in an immediate occupation of the conduction band at $\overline{K}$ followed by an ultrafast transfer (< 50 fs) to the conduction band minimum at $\overline{\Sigma}$. Both signals, at $\overline{K}$ and $\overline{\Sigma}$, do not vanish over the observed period of 400 fs. The technique described here enables direct access to the charge transfer dynamics in k-space and allows the study of decay times and decay channels in various systems with dependence on the excess energy or helicity of the excitation.

Transition-Metal Dichalchogenides (TMDC's) have been widely studied because of their rich phase diagram that includes superconductivity, charge-density waves or metal insulator transitions. With the recent emergence of TMDC atomically thin films [1, 2], the interest in these materials has increased dramatically also due to potential applications, like switching and optoelectronic devices [3, 4], energy storage [5] or nanodevices [6]. Heterostructures of MoS_2 and graphene or other TMDC materials add another degree of freedom to tailor material properties and are an important step toward functional devices [7–9]. Despite the tremendous efforts in this field, there still remains strong disagreement on fundamental properties. Measurements of carrier mobilities, for example, differ by one order of magnitude [3, 10] and decay times extracted from time-resolved absorption measurements even differ by up to two orders of magnitude [11–13]. In the case of monolayer films, many of these discrepancies may be related to the influence of the substrate or sample quality. However, even for bulk or few-layer samples, electron relaxation processes are not fully understood and only a small number of time-resolved experiments have been reported [14, 15]. A common problem of many experiments is the indirect nature of the measurements. In pure optical experiments, for example, many possible excitation and relaxation pathways can contribute to the measured transients which makes the identification of transfer and decay channels difficult.

For single-crystalline samples, time- and angle-resolved two-photon photoemission (2PPE) can provide this information in many cases as it is capable of directly imaging the electron dynamics in k-space [16, 17]. Electronic states at surfaces and in two-dimensional or layered materials are delocalized in two directions and well localized in the perpendicular direction. The excited electrons are then characterized by their energy and parallel momentum, i.e. quantities that 2PPE accesses directly by measuring the kinetic energy E_{kin} and emission angle θ of the photoelectrons, just like standard angle-resolved photoemission (ARPES) of occupied states. In contrast to ARPES, angle-resolved 2PPE is often limited to the detection of small parallel momenta ($\lesssim 0.5$ Å^{-1}) around $\overline{\Gamma}$ since it typically employs photon energies only up to 6.5 eV which can be generated in available nonlinear crystals [18–20]. It can be seen easily from the relationship $k_{\parallel}(\mathring{A}^{-1}) = 0.514\sqrt{E_{kin}(eV)}\sin\theta$ that photon energies of 20 eV and higher are required in order to probe the full Brillouin zone of typical materials.

High harmonic generation (HHG) in noble gas jets makes it possible to produce ultrashort

pulses in this energy range and utilize them for time-resolved photoemission experiments [16, 21]. First angle-resolved 2PPE experiments with high-harmonic probe studied collective phenomena after strong excitations in the occupied band structures such as phase transitions in charge-density wave materials and magnetic systems [22–24] or hot electron dynamics close to the Fermi level E_F as in graphene [25, 26]. In these experiments, the specific photon energy of the excitation played a minor role. Only recently, an example has been shown where, for a sub-monolayer of MoS_2 on an Au(111) substrate, tunable pump pulses were used to drive a specific transition into unoccupied bands far above E_F [27]. This is also the only study on a MoS_2 based system in which the ultrafast excitation and decay at the $\overline{K}$ point have been directly observed. All of the aforementioned experiments were based on laser systems with high pulse energies at repetition rates in the few kHz regime which make it easy to reach the high intensities that are required for HHG. The signal-to-noise ratio in photoemission spectroscopy, however, greatly benefits from higher repetition rates which also reduce space charge effects that are not only relevant for the high-harmonic probe pulses [28], but also for the pump pulses [29]. In addition, the applied pump fluence has to be limited if we want to study single-particle dynamics rather than collective processes, making a higher repetition rate even more desirable.

In this letter, we demonstrate that 2PPE experiments with HHG probe pulses are feasible at high repetition rates and charge transfer after excitation to the conduction band with visible pump pulses can be directly mapped in k-space. We chose bulk MoS_2 as a prototypical example for the observation of charge transfer dynamics in k-space. For this material, a direct transition at $\overline{K}$ is accessible with our pump pulses and the transfer to the conduction band minimum at the $\overline{\Sigma}$ point is suggested by many experimental and theoretical studies. The experiments were carried out on a setup which has been developed in our group [30]. A sketch is shown in Fig. 1. It combines a high-repetition rate laser system for high-harmonic generation, tunable pump pulses in the visible regime, and a 3D electron spectrometer which is capable of energy and k_x,k_y-momentum mapping in both directions parallel to the surface. The output of a 800 nm, 50 fs, 100 kHz, 1 W regenerative amplifier is split 50/50 into one pump and one probe arm. Pump pulses are frequency converted by an optical parametric amplifier, which is tunable between 480 and 700 nm, with a typical pulse energy of 200 nJ. The pump beam is focused outside the UHV chamber by an $f = 500$ mm spherical mirror and redirected inside the UHV by a cutted mirror to enter the analyzer chamber almost

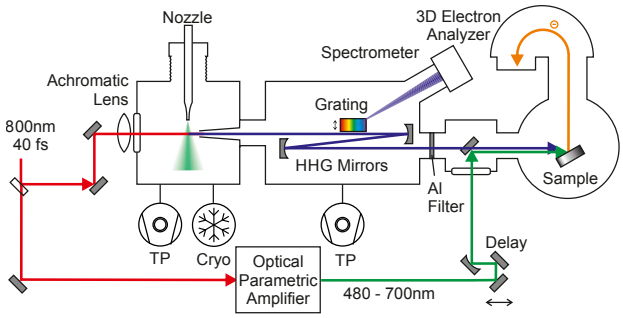

FIG. 1. Sketch of the experimental setup. Pump pulses are frequency converted by an optical parametrical amplifier. Probe pulses are focused into a Xe-jet and the generated harmonics are selected by two multi-layer mirrors. Both pulses are overlapped before entering the analyzer chamber equipped with a Scienta DA30 hemispherical analyzer.

collinear with the HHG-beam. With a spot size well below 200 μm, we achieved pump fluences up to 1 mJ/cm^2.

The generation of high harmonics in this setup is explained in great detail in [30]. Here, we summarize the most important points for this experiment and significant improvements. The laser pulses of the probe arm are focused by an achromatic $f = 60$ mm lens into a Xenon gas jet in an ultrahigh vacuum chamber generating high harmonics up to the 21$^{\text{st}}$ harmonic of the fundamental. The Xenon gas jet is generated by a glass nozzle with an inner diameter of 30 μm at a backing pressure of 4 bar. An additional cryopump not only increases pumping speed in the jet chamber, but also enables us to efficiently recycle the Xenon. While operating the jet, we connect the output of the turbo pump to the cryopump and are thereby able to freeze all of the used Xenon within the cryopump. After continuous operation over several days, the Xenon is then defrosted into a 50 l stainless steel vessel and liquified in a half liter gas cylinder cooled by liquid nitrogen. From this procedure, we are able to recycle almost all of the used Xenon.

In order to characterize and optimize the harmonic spectrum, a grating (600 lines/mm) can be moved into the beam and the diffraction pattern is detected on a multichannel plate with a phosphorus screen. The calibration of the HHG intensity was done by extrapolating single-photon counts at low intensities taking into account the efficiency of the grating and the MCP as well as the transmission through the filter for an absolute value of the number of photons per second. By varying the distance of the nozzle from the focus, both along and

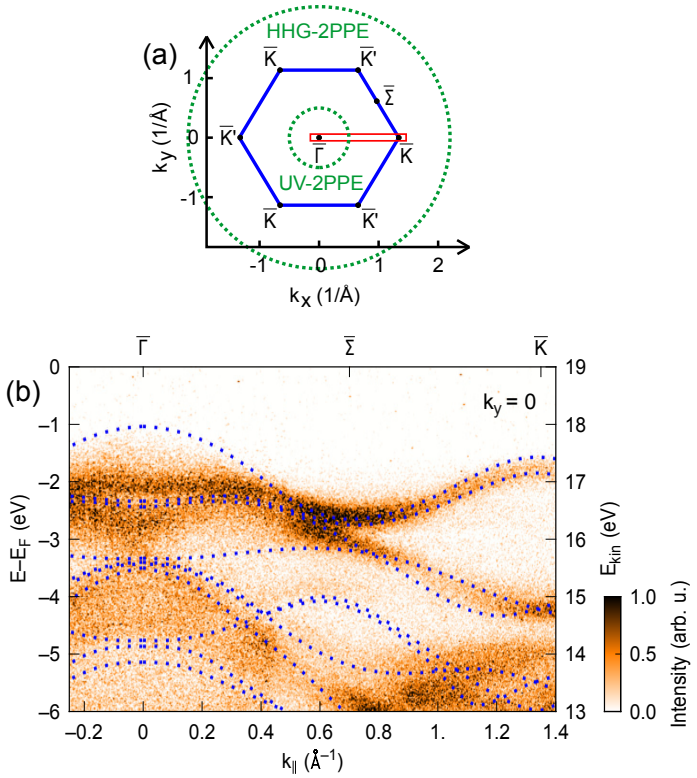

FIG. 2. (a) Brillouin zone of MoS_2 with important high symmetry points. Measurements were carried out along $\overline{\Gamma} - \overline{K}$ as indicated by the red bar. Dashed green lines illustrate the increase in observable parallel momentum when using probe pulses generated by high harmonics (HHG-2PPE) in contrast to typical UV pulses (UV-2PPE). (b) Measured energy-momentum map in the $\overline{\Gamma} - \overline{K}$ direction. Blue dashed lines are theoretical band structure calculations.

perpendicular to the optical axis, as well as the gas pressure, we are able to optimize the flux of a specific harmonic. We achieved the highest overall flux of $> 10^{10}$ photons/s for the 15^{th} harmonic (23.25 eV). In order to select a single harmonic, we use a pair of multi-layer mirrors (IOF Jena) with a reflectivity of larger than 30% while suppressing about 99% of neighboring harmonics. The accessible momentum space for this photon energy is illustrated in Fig. 2a where the Brillouin zone of MoS_2 is drawn in blue. Green dashed circles indicate the photoemission horizon for a typical 2PPE using UV probe pulses (inner circle) and HHG at 23.25 eV (outer circle).

Commercial 2H-MoS_2 single crystals (2D Semiconductors) were cleaved *in situ* under ultra high vacuum conditions at a pressure of better than 10^{-10} mbar. The orientation and surface quality was checked by means of LEED. We oriented all samples with the analyzer

slit parallel to the $\overline{\Gamma}-\overline{K}$ direction as indicated by the red rectangle in Fig. 2a in order to map the $\overline{\Sigma}$ and the $\overline{K}$-point within the same measurement at $k_y = 0$. All spectra are recorded at room temperature with a Scienta DA30 hemispherical analyzer. Fig. 2b shows the recorded two-dimensional energy versus momentum maps in this direction, excited solely with the HHG pulses. The measured band structure is in very good agreement with theoretical calculations, taken from [31] (blue dashed lines). The absence of spectral weight in the valence band at the $\overline{\Gamma}$-point has been observed in ARPES measurements before [31, 32] and is attributed to a matrix element effect. We observe the spin splitting of the valence band at $\overline{K}$ when choosing a smaller entrance slit (0.5 mm) of the hemispherical analyzer (not shown). Since the time-resolved measurements are more limited by count rate than by energy resolution, we usually measure at large slit settings (2.5 mm).

Fig. 3a shows a sketch of the excitation process used for the time-resolved measurements. We pump with 600 nm (2.05 eV) photons, which is at least 200 meV above the A exciton resonance excitation. While the exciton binding energy in monolayer MoS_2 is predicted by theory to be up to 1 eV [33], experiments on bulk sample report a value of less than 100 meV [34]. We therefore expect for the optical excitation an interband transition from the valence to the conduction band close to the $\overline{K}$-point. After excitation, the electrons can subsequently decay to $\overline{\Sigma}$ where the global conduction band minimum is predicted by all band structure calculations. Our time-resolved experiments show this transfer directly. Only recently, this transfer has also been observed in the very similar material WSe_2 [35].

While for the band structure map shown in Fig. 2b three spectra were stitched together in order to cover the complete momentum path from $\overline{\Gamma}$ to $\overline{K}$, for the time-resolved measurements we chose a sample orientation where we can measure a single energy map that includes both $\overline{K}$ and $\overline{\Sigma}$. In Fig. 3 we show two of such energy maps at different delay times, before the excitation (negative delay) (b) and at temporal overlap (c). Both spectra were combined from measurements of the occupied states and unoccupied states, while the unoccupied part has been intensified by a factor of ~ 60 for better visibility. Each spectrum was measured for 30 min. Clearly, the population of the conduction band at the $\overline{K}$-point can be observed at temporal overlap even in the raw data. The part of the intensity distribution in the unoccupied part, which is also visible at negative delays, can be assigned to the residual neighboring 17^{th} harmonic. In this case, replica of the occupied band structure are shifted by 3.1 eV and superimpose the unoccupied part. This particularly applies for the

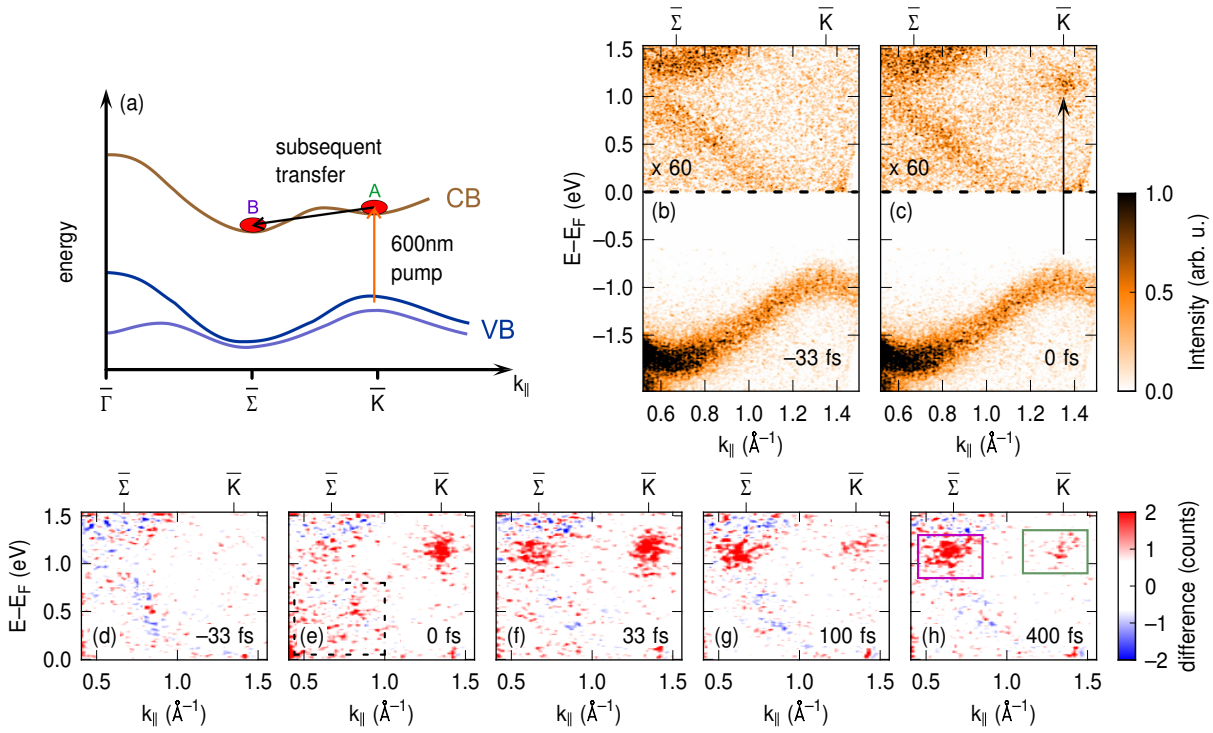

FIG. 3. (a) Excitation scheme of the experiment. Electrons are excited at $\overline{K}$ by pump pulses of 600 nm slightly above the A exciton resonance. They are subsequently transferred to the conduction band minimum at $\overline{\Sigma}$. (b) and (c) show energy-momentum maps before and at temporal overlap of the two laser pulses, respectively. Each map is composed of measurements of the occupied in the lower part and the unoccupied part in the upper part, separated by the Fermi energy (dashed black line). The intensity of the unoccupied part is amplified by a factor of ~ 60. The transiently populated conduction band in the latter case is clearly visible. (d)-(h) Difference spectra at various time delays for illustration of the charge transfer. Even for the longest delay (h) the population at $\overline{K}$ remains visible. Additional intensity around temporal overlap in the lower left corner is assigned to non-resonant excitation.

$\overline{\Sigma}$-point, where we expect the signature of the subsequently transferred electrons. In order to suppress this background, we subtract the energy map at negative delay from each energy map of the subsequent time steps. In addition, these spectra are rebinned by a factor of 8 x 8. These difference spectra, which are shown in Fig. 3d-h, solely represent the transiently excited electron distribution. In order to account for laser drift during the measurement, we have repeated the delay scan 10 times with an integration time of 5 min for each time step

resulting in a total acquisition time of 16 hours.

The difference spectrum in Fig. 3e shows the intensity right at the optical excitation at $\overline{K}$. It can now be clearly seen that already after one time step of 33 fs after the optical excitation (Fig. 3f), a significant population has been built up at the $\overline{\Sigma}$-point. This is a significantly faster transfer time compared to results deduced from pure optical experiments [15]. Remarkably, the population at both points in the conduction band do not disappear even for delays up to 400 fs (Fig. 3h), the longest delay measured in this experiment. We observe an additional broad electron distribution in the lower left corner of Fig. 3e, which rapidly decays within the following two time steps. We assign this intensity to a direct two-photon transition from the occupied valence band around the $\overline{\Sigma}$ point without the population of an intermediate state. Such non-resonant 2PPE is well known from surface states of metals and its time-dependent signal has frequently been used to precisely determine the cross-correlation between pump and probe pulse directly on the sample in UHV [36, 37]. Similarly, we can use the transient of the region indicated by the black dotted box as cross-correlation between the visible pump and the HHG probe, which has a full width at half maximum of 80 fs.

Fig. 4 shows the temporal evolution of the electron intensities at $\overline{\Sigma}$ (green) and $\overline{K}$ (violet) and of the non-resonant 2PPE (black). The corresponding integration areas are depicted in Figs. 3e and h. After the optical excitation, the signal at $\overline{K}$ decays first on an ultrafast time scale and then remains almost constant over the observed period. It is clear that at least two states have to be involved in the decay mechanism, one, which decays with a time constant of $\approx$ 30 fs, and one long-lived in the picosecond range. The signal at $\overline{\Sigma}$ shows an ultrafast increase and decays with a time constant indistinguishable from the long-lived signal at $\overline{K}$. To understand the transfer mechanism in detail, further experiments are necessary. A theoretical work suggests that the transfer time depends on the excess energy of the excitation [**?**]. With our excess energy of at least 200 meV, we assume to be on the fast limit of the transfer. Direct filling of this state at $\overline{\Sigma}$ from the valence band is not possible with our excitation energy due to the significantly larger gap.

In conclusion, we have presented a direct mapping of the charge transfer in bulk MoS_2 from the $\overline{K}$ to the $\overline{\Sigma}$ point by time- and angle-resolved two-photon photoemission with HHG probe pulses. We are able to extract a transfer time well below 50 fs, when exciting the system slightly above the A exciton resonance. This is one order of magnitude faster than

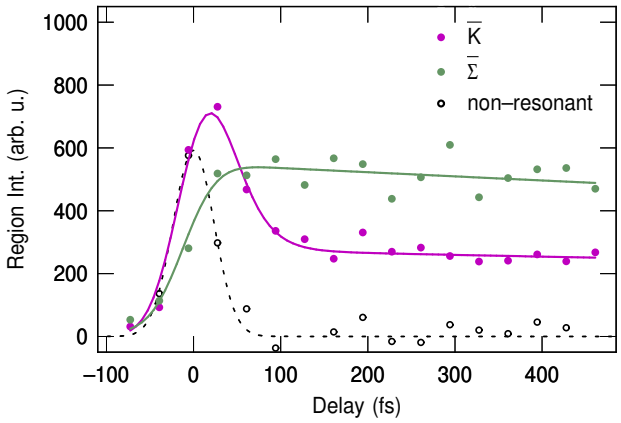

FIG. 4. Temporal evolution of the electron intensities in the two regions indicated by green and violet boxes in figure 3h. After excitation, the signal at $\overline{K}$ decreases almost on the same time scale as it increases while some longer lived signal remains. The intensity at $\overline{\Sigma}$ saturates already after one time step of 33 fs and then remains constant over the measured time interval. The cross-correlation of the laser pulses deduced from the the non-resonant signal close to Σ is indicated in black.

transfer times reported previously. In both regions, $\overline{\Sigma}$ and $\overline{K}$, a long-lived population remains in the conduction band with time constants of several ps. Our experimental technique enables many possible applications. The aforementioned dependence of the transfer time on the excess energy of the excitation [38] becomes accessible with the tunability of our pump pulses. On the other hand, it seems very promising and feasible to observe the charge transfer after spin-selective excitation of the distinct $\overline{K}$ and $\overline{K}'$ points using circularly polarized pump pulses even in bulk samples [39, 40]. With a 3D analyzer, it is even possible to access different high symmetry points at the same time without moving the sample and thereby observe the charge distribution in the non-equivalent $\overline{\Sigma}$ and $\overline{\Sigma}'$ points. By exciting the system on and above resonance, signatures of the exciton should be observable in the photoelectron distribution which would enable to address many open questions concerning the exciton dynamics in these materials. Particulary in the case of van der Waals heterostructures different relaxation pathways which are indistinguishable in real space could be traced in momentum space.

We gratefully acknowledge funding by the Deutsche Forschungsgemeinschaft through the SFB 1083. We thank C. Heyl for valuable discussion concerning the improvement of the

high-harmonic generation.

[1] K. F. Mak, C. Lee, J. Hone, J. Shan, and T. F. Heinz, Phys. Rev. Lett. **105**, 136805 (2010).

[2] A. Splendiani, L. Sun, Y. Zhang, T. Li, J. Kim, C.-Y. Chim, G. Galli, and F. Wang, Nano Lett. **10**, 1271 (2010).

[3] B. Radisavljevic and A. Kis, Nat. Mat. **12**, 815 (2013).

[4] Z. Yin, H. Li, H. Li, L. Jiang, Y. Shi, Y. Sun, G. Lu, Q. Zhang, X. Chen, and H. Zhang, ACS Nano **6**, 74 (2012).

[5] S. Ding, D. Zhang, J. S. Chen, and X. W. D. Lou, Nanoscale **4**, 95 (2012).

[6] W. Wu, L. Wang, Y. Li, F. Zhang, L. Lin, S. Niu, D. Chenet, X. Zhang, Y. Hao, T. F. Heinz, J. Hone, and Z. L. Wang, Nature **514**, 470 (2014).

[7] Y. Shi, W. Zhou, A.-Y. Lu, W. Fang, Y.-H. Lee, A. L. Hsu, S. M. Kim, K. K. Kim, H. Y. Yang, L.-J. Li, J.-C. Idrobo, and J. Kong, Nano Lett. **12**, 2784 (2012).

[8] X. Duan, C. Wang, J. C. Shaw, R. Cheng, Y. Chen, H. Li, X. Wu, Y. Tang, Q. Zhang, A. Pan, J. Jiang, R. Yu, Y. Huang, and X. Duan, Nat. Nanotechnol. **9**, 1024 (2014).

[9] A. K. Geim and Grigorieva, Nature **499**, 419 (2013).

[10] J. H. Strait, P. Nene, and F. Rana, Phys. Rev. B **90**, 245402 (2014).

[11] M. Seo, H. Yamaguchi, A. D. Mohite, S. Boubanga-Tombet, J.-C. Blancon, S. Najmaei, P. M. Ajayan, J. Lou, A. J. Taylor, and R. P. Prasankumar, Sci. Rep. **6**, 21601 (2016).

[12] E. M. Mannebach, K.-A. N. Duerloo, L. A. Pellouchoud, M.-J. Sher, S. Nah, Y.-H. Kuo, Y. Yu, A. F. Marshall, L. Cao, E. J. Reed, and A. M. Lindenberg, ACS Nano **8**, 10734 (2014).

[13] H. Shi, R. Yan, S. Bertolazzi, J. Brivio, B. Gao, A. Kis, D. Jena, H. G. Xing, and L. Huang, ACS Nano **7**, 1072 (2013).

[14] A. Tanaka, N. J. Watkins, and Y. Gao, Phys. Rev. B **67**, 113315 (2003).

[15] N. Kumar, J. He, D. He, Y. Wang, and H. Zhao, J. Appl. Phys. **113**, 133702 (2013).

[16] R. Haight, Surf. Sci. Rep. **21**, 275 (1995).

[17] M. Rohleder, K. Duncker, W. Berthold, J. Güdde, and U. Höfer, New J. Phys. **7**, 103 (2005).

[18] N. H. Ge, C. M. Wong, R. L. Lingle, J. D. McNeill, K. J. Gaffney, and C. B. Harris, Science **279**, 202 (1998).

[19] W. Berthold, U. Höfer, P. Feulner, E. V. Chulkov, V. M. Silkin, and P. M. Echenique, Phys.

Rev. Lett. **88**, 056805 (2002).

[20] F. Schmitt, P. S. Kirchmann, U. Bovensiepen, R. G. Moore, L. Rettig, M. Krenz, J. H. Chu, N. Ru, L. Perfetti, D. H. Lu, M. Wolf, I. R. Fisher, and Z. X. Shen, Science **321**, 1649 (2008).

[21] M. Bauer, C. Lei, K. Read, R. Tobey, J. Gland, M. M. Murnane, and H. C. Kapteyn, Phys. Rev. Lett. **87**, 025501 (2001).

[22] T. Rohwer, S. Hellmann, M. Wiesenmayer, C. Sohrt, A. Stange, B. Slomski, A. Carr, Y. Liu, L. M. Avila, M. Kallne, S. Mathias, L. Kipp, K. Rossnagel, and M. Bauer, Nature **471**, 490 (2011).

[23] J. C. Petersen, S. Kaiser, N. Dean, A. Simoncig, H. Y. Liu, A. L. Cavalieri, C. Cacho, I. C. E. Turcu, E. Springate, F. Frassetto, L. Poletto, S. S. Dhesi, H. Berger, and A. Cavalleri, Phys. Rev. Lett. **107**, 177402 (2011).

[24] B. Frietsch, R. Carley, K. Döbrich, C. Gahl, M. Teichmann, O. Schwarzkopf, P. Wernet, and M. Weinelt, Rev. Sci. Instr. **84**, 075106 (2013).

[25] I. Gierz, F. Calegari, S. Aeschlimann, M. Chávez Cervantes, C. Cacho, R. T. Chapman, E. Springate, S. Link, U. Starke, C. R. Ast, and A. Cavalleri, Phys. Rev. Lett. **115**, 086803 (2015).

[26] J. C. Johannsen, S. Ulstrup, F. Cilento, A. Crepaldi, M. Zacchigna, C. Cacho, I. C. E. Turcu, E. Springate, F. Fromm, C. Raidel, T. Seyller, F. Parmigiani, M. Grioni, and P. Hofmann, Phys. Rev. Lett. **111**, 027403 (2013).

[27] A. Grubišić Čabo, J. Miwa, S. S. Grønborg, J. M. Riley, J. C. Johannsen, C. Cacho, O. Alexander, R. T. Chapman, E. Springate, M. Grioni, J. V. Lauritsen, , P. D. C. King, P. Hofmann, and S. Ulstrup, Nano Lett. **15**, 5883 (2015).

[28] S. Passlack, S. Mathias, O. Andreyev, D. Mittnacht, M. Aeschlimann, and M. Bauer, J. Appl. Phys. **100**, 024912 (2006).

[29] L.-P. Oloff, K. Hanff, A. Stange, G. Rohde, F. Diekmann, M. Bauer, and K. Rossnagel, J. Appl. Phys. **119**, 225106 (2016).

[30] C. M. Heyl, J. Güdde, A. L'Huillier, and U. Höfer, J. Phys. B **45**, 074020 (2012).

[31] D. W. Latzke, W. Zhang, A. Suslu, T.-R. Chang, H. Lin, H.-T. Jeng, S. Tongay, J. Wu, A. Bansil, and A. Lanzara, Phys. Rev. B **91**, 235202 (2015).

[32] T. Böker, R. Severin, A. Müller, C. Janowitz, R. Manzke, D. Voß, P. Krüger, A. Mazur, and J. Pollmann, Phys. Rev. B **64**, 235305 (2001).

[33] D. Y. Qiu, F. H. da Jornada, and S. G. Louie, Phys. Rev. Lett. **111**, 216805 (2013).

[34] N. Saigal, V. Sugunakar, and S. Ghosh, Appl. Phys. Lett. **108**, 132105 (2016).

[35] R. Bertoni, C. W. Nicholson, L. Waldecker, H. Hübener, C. Monney, U. De Giovannini, M. Puppin, M. Hoesch, E. Springate, R. T. Chapman, C. Cacho, M. Wolf, A. Rubio, and R. Ernstorfer, ArXiv e-prints (2016), 1606.03218.

[36] T. Hertel, E. Knoesel, M. Wolf, and G. Ertl, Phys. Rev. Lett. **76**, 535 (1996).

[37] I. L. Shumay, U. Höfer, C. Reuß, U. Thomann, W. Wallauer, and T. Fauster, Phys. Rev. B **58**, 13974 (1998).

[38] A. Steinhoff, M. Florian, M. Rösner, M. Lorke, T. O. Wehling, C. Gies, and F. Jahnke, 2D Mater. **3**, 031006 (2016).

[39] J. M. Riley, F. Mazzola, M. Dendzik, M. Michiardi, T. Takayama, L. Bawden, C. Granerod, M. Leandersson, T. Balasubramanian, M. Hoesch, T. K. Kim, H. Takagi, W. Meevasana, P. Hofmann, M. S. Bahramy, J.W.Wells, and P. D. C. King, Nat. Phys. **10**, 835 (2014).

[40] X. Zhang, Q. Liu, J.-W. Luo, A. J. Freeman, and A. Zunger, Nat. Phys. **10**, 387 (2014).